School of Mathematical
and Physical Sciences

University of Reading

Department of Mathematics and Statistics

Preprint MPS-2011-12

07 October 2011

Superfast non-linear diffusion model of capillary transport in particulate porous media

by

A.V. Lukyanov, M.M. Sushchikh, M.J. Baines and T.G. Theofanous

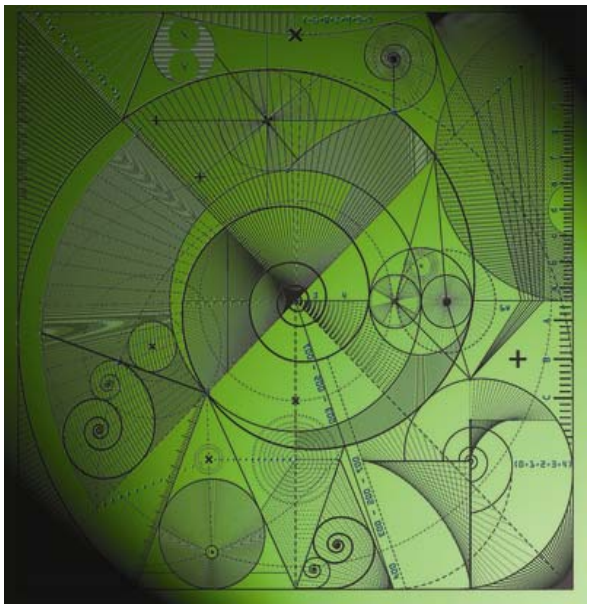

Superfast non-linear diffusion model of capillary transport in particulate porous media.

A.V. Lukyanov[1], M.M. Sushchikh[2], M.J. Baines[1], T.G. Theofanous[2]

Department of Mathematics and Statistics, University of Reading, Reading RG6 6AX, U.K.[1]

Center for Risk Studies and Safety, University of California at Santa Barbara, Santa Barbara, CA, USA.[2]

Abstract

The migration of liquids driven by the capillary forces in a network of particulate porous medium, such as sand, usually occurs through the voids between the particles at high saturation levels. In this letter we study a special regime, at low and very low saturation levels, when the transport of liquids can only take place over the rough surface elements of the constituent particles connected by the capillary bridges formed between them. We demonstrate, both experimentally and theoretically, that this migration or spreading is actually a complex interplay between capillary bridges and the liquid film situated on the rough surface area of the particles, which manifests itself macroscopically as a rather special case of diffusion, a superfast nonlinear diffusion process, which has been previously found only in a few applications in plasma physics. We propose a simple, but universal, model of this phenomenon and compare predictions with our experiments.

Non-volatile persistent liquids can spread significantly in porous substrates and cover large areas for long periods of time before they are removed by evaporation. For example, we found in experiments that a single 0.01 ml drop of trioctyl-phosphate (TEHP) with a saturated vapour pressure at room temperature of $P_s \simeq 10^{-5}\,\mathrm{Pa}$ (such low pressure guarantees the absence of evaporation effects and persistence over a period of tens of days) may spread over $V_s \simeq 6$ ml volume in ordinary sand. These numbers suggest that the saturation level $s = V_l/V_v$, defined as the ratio of the total specific liquid volume V_l to the specific volume of voids in sand V_v, should have been about $0.6\,\%$ when the wet volume reached V_s. It is intuitively obvious, assuming the liquid partially wets the sand, that this amount may be totally accommodated on the rough surface of the particles. But what happens before such low levels are reached, how quickly may this happen, how far may this spreading process go, and in general how different is this regime in comparison to the well-studied process of penetration at high saturation levels? To answer those questions, we propose a macroscopic model describing transport at low levels of saturation s and compare it with some of our experiments.

To understand the distinctive features of this low saturation level regime, we first consider the morphology of the liquid domains accommodated in a porous matrix consisting of spherical beads, the case which has been investigated in detail previously [1–3] in the context of the mechanical properties of wet granular materials. It has been found that, depending on the

saturation level, the liquid domains may either take the form of isolated pendular rings, or simply liquid bridges, formed between the spherical particles at the points of contact at $s_{min} < s < 7 - 8\%$, or they may coalescence into more complex structures like trimers, pentamers and heptamers at higher saturation levels ($8\% < s < 24\%$) [1–2], Fig. 1. If the saturation level increases any further, larger clusters are formed, such that finally at $s \approx 33\%$ one can find that the largest cluster comprises of about 90% of the entire volume of the liquid in the porous matrix. The minimal value of the saturation, s_{min}, at the onset of the capillary bridge network, is found to be about $s_{min} \simeq 0.2\%$, [3], and is conditioned, to preserve connectivity of the network, by the minimum volume of the pendular ring, which is defined by the roughness of the particle surface.

Therefore it may be anticipated that we have at least two regimes of spreading in particulate materials. This is along the lines of similar classifications, which may be found in the studies of the moisture saturation levels in natural ice and industrial powders [3–4]. The first regime (also called the pendular regime), which we are mostly interested in here, lies in the range $s_{min} < s < 24\%$, when the transport of liquids may only occur over the surfaces of the constituent particles. In the second regime (also known as the funicular regime) above the critical value of $s \simeq 24\%$, the liquid domain is almost continuous everywhere and the penetration process has a character of multiphase flow, which has been previously studied in soil sciences [6].

The surface of the particles is never perfect and part of the liquid accommodated in the porous matrix is found inside the grooves of the surface roughness. So the liquid content or saturation s should actually be split into two contributions, $s = s_p + s_r$, where s_p is the liquid inside the bridges and s_r is the liquid in the film covering the rough surface of the particles. As such, the process of migration of liquids in particulate porous media is actually an interplay between those two components, and the surface roughness plays a crucial role.

The structure of porous systems is usually very complex and, even in the case of identical spherical particles, rather difficult to model in detail. So we follow Darcy's macroscopic approach, which is formulated in terms of the dynamics of approximated continuous distributions of macroscopic pressure p, velocity $\mathbf{v}$ and the saturation, s, which are interrelated via Darcy's Law relating liquid flux $\mathbf{q} = \phi s \mathbf{v}$ and the gradient of capillary pressure $p_c(s)$, i.e.

$$\mathbf{q} = -\frac{k(s)}{\mu} \left(\nabla p_c - \rho g_0 \mathbf{e}_z \right). \tag{1}$$

together with the equation of continuity

$$\frac{\partial \phi\, s}{\partial t} + \nabla(\phi\, s\mathbf{v}) = 0, \tag{2}$$

where μ and ρ are the viscosity and density of the liquid, $k(s)$ and $\phi(s)$ are the permeability and porosity of the porous network and g_0 is the acceleration due to gravity acting in the z-direction, [6]. All the specific information about the particular porous system and associated

complex non-linear behaviour is contained in the functional parameters of the Darcy law, that is the coefficient of permeability $k(s)$, which is the measure of resistance to the flow, and the gradient of capillary pressure $p_c(s)$, which is the driving force. On this basis several different models have been developed over the years for the needs of petroleum engineering and soil science [6]. For simplicity, we further neglect the contribution from gravity, assuming effectively that the Bond number $\rho g_0 L^2/\sigma << 1$, where σ is the coefficient of surface tension and L is the length scale of the system.

For any macroscopic elementary volume in the porous matrix, one can in principle relate the average pressure with the average amount of liquid contained in the capillary bridges, and thus with the saturation s. In the case of identical spheres (though not only) a relationship between the volume of the bridge (the pendular ring) and the mean curvature of the free surface of the bridge is available in an analytical although rather complex form [7]. Some typical dependencies obtained numerically from the formulae derived in [7] in the gravity free case and negative mean curvature range are illustrated in Fig. 2b for the geometry shown in Fig. 2a, as functional dependences of the normalised mean curvature of the free surface HR_0 on the normalised bridge volume $V_p R_0^{-3}$, where R_0 is the mean particle radius. Note that the case of two smooth identical spheres in contact is equivalent to $D = 0$ and $\theta_2 = \pi/2$, Fig. 2a. In the case of almost complete wetting liquid - solid combinations, that is when the apparent contact angle $\theta_1 \approx 0$, the best fit to that dependence is given by

$$HR_0 = C_0 - C_1 (V_p R_0^{-3})^{\gamma} \tag{3}$$

with $\gamma \approx -0.5$, $C_1 \approx 1.3$, $C_0 \approx 4$, which is consistent with the estimates obtained in [3].

In developing the model, we concentrate on the case of $\theta_1 \approx 0$ and take the fit given by (3) as the typical example, although, we note that it is still assumed that $\theta_1 > 0$. The regime of complete wetting at $\theta_1 = 0$ is a special one, which is controlled by the gradient of disjoining pressure. Some aspects of this special regime have been studied in [8], where it has been established that dispersion in porous media at low complete wetting phase saturations is actually a hyperdispersion, which may lead to anomalously fast spreading.

Now, the saturation s can be linked with the capillary pressure $p_c = 2\sigma H$. Indeed, $s_p = \alpha_p^{-1} V_p R_0^{-3}$, where $\alpha_p = \frac{4\pi}{3N_c}\frac{\phi}{1-\phi}$, N_c being the coordination number of the liquid bridges, which lies between 4 and 8 according to the results obtained in [3] and our experimental observations using X-ray microtomography in sands. So, $s = \alpha_p^{-1} V_p R_0^{-3} + s_r$, and thus

$$p_c(s) = \frac{2\sigma}{R_0}\left\{C_0 - C_1\,\alpha_p^{\gamma}(s - s_r)^{\gamma}\right\}. \tag{4}$$

It is obvious, in general, that the coefficient of permeability, which appears in (1), is essentially defined by the properties of the surface roughness, since the liquid flux in the low

saturation regime only occurs over the surface elements of the grains. While general theoretical analysis of wetting flows over rough surfaces is essentially incomplete, one can obtain an estimate of the permeability coefficient on the basis of results for a special case of capillary flows in open V-shape channels. It has been found [9–10] that in this case the liquid content is almost independent of the capillary pressure provided that $|p_c| < \frac{2\sigma}{h_0}$, where h_0 is the height of the groove. If we now associate the size of the capillary channel h_0 with the characteristic value, ΔR_0, of the local surface departure from the mean spherical shape of the grain particle of radius R_0, then at $|p_c| < \frac{2\sigma}{\Delta R_0}$ the liquid content on the rough surface of the particles in porous matrix may be considered approximately as constant, and so are the coefficients $k(s) \approx const$, $s_r(s) \approx const$. Then their upper bound can be estimated as follows. The number of closely packed capillary channels of size ΔR_0 and cross sectional surface area $S_c = \Delta R_0^2/2$ on the perimeter of a spherical particle is $N_R = 2\pi R_0/\Delta R_0$. The flux through those capillaries is on average passing through a surface area of $S_0 = 4R_0^2$ in the porous matrix, while the flux in each capillary $q_c \cong \frac{S_c^2}{8\pi\mu}\Delta P$, ΔP is the pressure difference, [9–10]. Then the average permeability coefficient would be of the order of $k(s) = const = k_0 \approx \frac{N_R S_c^2}{8\pi S_0} = \frac{\Delta R_0^3}{256 R_0}$. In principle, this value should also include a correction for tortuosity, $0 < c_T < 1$, so that $k_0 \approx c_T \frac{\Delta R_0^3}{256 R_0}$. At the same time $s_r(s) = s_r^0 \approx \frac{1-\phi}{\phi}\,\frac{3\Delta R_0}{2R_0}$. These are the main assumptions in our model. More accurate estimation of the permeability and the film content as a function of s would need further analysis of the flows over rough, and essentially curved surfaces, in the connected porous matrix.

Now, using (4) and assuming uniform porosity ϕ, one can cast (1) and (2) into a single non-linear diffusion equation,

$$\frac{\partial s}{\partial t} = D_0 \nabla \left(\frac{\nabla s}{(s - s_r^0)^{1-\gamma}} \right), \tag{5}$$

where

$$D_0 = \frac{2\sigma}{R_0}\frac{k_0}{\mu}\frac{C_1|\gamma|\alpha_p^\gamma}{\phi}.$$

Equation (5) should be complemented with the boundary condition $s = s_F > s_r^0$ at the front moving with the Darcy velocity

$$\mathbf{v} = -D_0 \frac{\nabla s}{s(s - s_r^0)^{1-\gamma}}.$$

Changing to a new variable $\tilde{s} = s - s_r^0$, one can transform (5) into

$$\frac{\partial \tilde{s}}{\partial t} = D_0 \nabla \left(\frac{\nabla \tilde{s}}{\tilde{s}^{1-\gamma}} \right). \tag{6}$$

Equation (6) for $\gamma < 0$ belongs to the so called superfast class of non-linear diffusion equations, which has been previously found only in a few applications in plasma physics [11]. The principal difference in the behaviour of solutions between the standard porous medium equation (PME) (for $\gamma > 1$) and the superfast diffusion equation (SFDE) (for $\gamma < 0$) is the motion of the

front. In the case of PME, the small values of $\tilde{s} \approx 0$ at the front lead to the so called stagnation, for which $\mathbf{v} \approx 0$ and waiting times occur before the front effectively starts moving [12]. This is clearly not the case in SFDE problems, where, on the contrary, the front speed increases as the boundary value $\tilde{s}$ decreases. This may be illustrated if we consider a one-dimensional initial value problem for (6) on $x \in [0, \infty)$ with two boundary values $\tilde{s}(1,0) = \tilde{s}_F = 10^{-2}$ and $\tilde{s}_F = 5 \times 10^{-3}$, $D_0 = 1$, compactly support initial conditions $\tilde{s}(x,0) = \tilde{s}_F + (1 - \tilde{s}_F)\cos(\pi x/2)$ on $x \in [0,1]$ and two different values of $\gamma_1 = -0.5$, $\gamma_2 = 2$. The problem has been solved numerically by a semi-implicit moving-mesh method, [12]. Motion of the front and corresponding profiles of $\tilde{s}(x,t)$ for PME are shown in Figs. 3a,b, where one can see the delay time before the front starts moving faster. The SFDE case is illustrated in Figs. 3c, d. One can observe that the front propagation speed $\dot{x}(t)$ is much larger in the case of SFDE for the same parameter values as for PME and is growing with the $\tilde{s}_F$ decreasing.

Now, consider how this SFDE model agrees with experimental observations. As an example, we compare numerical solutions with the results of our experiments on the spreading of persistent liquids (with extremely low vapour pressure), such as trioctyl-phosphate (TEHP) and tricresyl-phosphate (TCP), in standard Ottawa (Illinois) F sand with an average grain size of $250\,\mu$m, porosity of 30% and surface roughness in the range $0.5 < \Delta R_0 < 3\,\mu$m [13]. The TEHP liquid has saturated vapour pressure at room temperatures $p_{vs} \simeq 1.1 \times 10^{-5}\,$Pa, [14], coefficient of surface tension $\sigma = 29 \pm 1\,$mN/m, measured in our laboratory at $25^\circ C$, viscosity $\mu \simeq 15\,$mPa$\cdot$s at $20^\circ C$, [15], and contact angles on a sufficiently smooth flat glass surface close to $\theta_1^s \approx 10^\circ$ and on a rough flat glass surface close to $\theta_1^r \approx 0^\circ$; both angles have been measured from the image of a liquid TEHP drop placed on the surfaces. In the experiment, the microliter drops of TEHP were deposited on naturally-packed sand beds, and the footprint of spreading on the surface of sand has been traced by ultraviolet (UV) fluorescence by adding Coumarin dye into the liquid. The experimental setup also included an embedded grid and a support-lowering mechanism, so as to capture and take measurements of the shape of the wetted portion of sand. We have found that the shape of the wetted portion of sand is close to a hemisphere, so that its volume can be easily calculated from the footprint radius with sufficient accuracy. The typical image of the footprint, obtained by a 10.7 MP digital camera with a macrolense being able to resolve single sand particles, is shown in Fig. 4. The camera has been fitted with a longpass coloured glass filter to suppress scattered UV light, such that no essential background signal has been detected in the absence of the dye in the range of camera gains used in the experiments. We have taken images at different values of the camera gain to ensure confident capture of the wetted front position. The typical evolution of the wetted volume $V(t)$, and the averaged over the volume saturation (calculated in the absence of evaporation from the mass conservation) are shown in Fig. 5 for an 11 microliter drop. One can clearly see the transition from the high saturation regime of spreading to the low saturation pendular regime at $s \simeq 30\%$

(at $t \approx 100$ min). The typical rate exponent of the second regime q_p, before the front reaches a "stagnation point", is found to be $V(t) \propto t^{q_p}$, $q_p^{TEHP} = 0.80 \pm 0.02$, Fig. 5. A similar value of $q_p^{TCP} = 0.785 \pm 0.015$ has been found in the case of spreading of another persistent liquid, TCP, with somewhat different physical properties, noticeably the coefficient of surface tension and the contact angles, $p_{vs} \simeq 8 \times 10^{-5}\,\mathrm{Pa}$, $\sigma = 42.5 \pm 1\,\mathrm{mN/m}$, $\mu \simeq 20\,\mathrm{mPa} \cdot \mathrm{s}$, $\theta_1^s \approx 30^\circ$, $\theta_1^r \approx 20^\circ$. As we will see further in the comparison, these values of q_p agree very well with the ones found in our numerical simulations of (5) in a three-dimensional case with parameters s_r^0, s_F relevant to our experimental conditions (parameter D_0 does not affect the rate exponent and can only rescale time t). One needs to emphasise that in general the rate exponent is a function of s_r^0, s_F in the model (5), that is a functional of the surface roughness and wettability properties. Although the results for the TCP case show that the parameters s_r^0, s_F may not be very sensitive to wettability as long as the contact angle is not too large. More detailed parametric study of the superfast model (5) will be reported elsewhere.

In making the comparison between experimental data and numerical solutions of the model, we use the symmetry of the wet region and solve equation (5) assuming that saturation $s = s(r)$ is a function of the radius of the domain only. The mathematical model has three independent parameters: D_0, s_F and s_r^0. The parameter s_F can be found from experiment at the "stagnation point" of the front, $s_F \simeq 0.6\%$, see Fig. 5. This value is smaller than $s_F \simeq 1.4\%$, which is what one would expect from the minimum $min(\Delta R_0) = 0.5\,\mu$m, and corresponds to an effective $(\Delta R_0)_e = 0.2\,\mu$m. The ratio $(s_F - s_r^0)/s_F << 1$, which is a measure of the capillary pressure at the front driving the spreading, can be obtained from the distribution of the amplitude of surface roughness, that is from $\max(\Delta R_0) = 3\,\mu$m. The minimum volume of the bridge before its rupture at the separation distance $D = \max(\Delta R_0)$ can be estimated from $\min(V_p R_0^{-3}) \simeq (2DR_0^{-1})^3$, [16]. This yelds $\min(s_p) = \alpha_p^{-1} \min(V_p R_0^{-3})$, which is in our case $\min(s_p)/s_F = (s_F - s_r^0)/s_F \simeq 0.1$. As a result we set $s_r^0 \simeq 0.9 s_F$, leaving D_0 as the only fitted parameter in the model. Note, that the value of D_0 can only scale time t in (5) but can not affect the rate exponent q_p. The unknown initial conditions are taken in the form $s(r,0) = s_F + (1 - s_F)\cos(\pi r/2)^\lambda$ on $r \in [0,1]$ with $1 < \lambda < 3$, the parameter, which is used for fine tuning only. In making the comparison we always start our simulations at low levels of averaged saturation, typically at $\int_0^1 s(r)\, r^2 dr \simeq 3 - 4\%$, which is usually reached after 20 hours of spreading. Note that at the same time the peak value of s could be three times higher. The results of simulations are shown in Fig. 6 for 11, 4.4 and 2.2 microliter drops. The parameter $D_0 = 10^{-14}$ has been determined to fit an 11 microliter drop volume spreading curve first, and then the set of parameters has been fixed to produce simulations for the two other cases with essentially smaller volumes of liquid. The value of the diffusion coefficient so obtained corresponds to the estimate for effective surface roughness amplitude $(\Delta R_0)_e \approx 0.2\,\mu$m at $c_T = 0.3$ and $N_c = 8$. Note that the parameter s_F has been fixed for all the cases, though it has shown some variations.

In conclusion, we have demonstrated that the process of liquid spreading at low and very low levels of saturation in granulated porous media is essentially a superfast diffusion process controlled by the surface roughness of the particles, which has very specific features separating it from other nonlinear diffusion processes. The mathematical model that we have derived has been verified on experiments with persistent liquids spreading without substantial evaporation effect and has shown very good potential to be a universal tool for evaluations of liquid spreading at low saturation levels. The model can be easily scaled down or up to describe transport in fine nanoparticle assembly or in coarse granular materials.

Acknowledgement. This work is supported by the Joint Science and Technology Office, US Defense Threat Reduction Agency (JSTO/DTRA), Threat Agent Science (TAS).

---

[1] M Scheel et al. (2008) Nature Materials 7 189–193.

[2] M Scheel et al. (2008) J. Phys. Condens. Matter 20 494236.

[3] S. Herminghaus (2005) Advances in Physics 54 221-261.

[4] S.L. Flemmer (1991) Powder Technology 66 191-194.

[5] A. Denoth (1999) Cold Regions Science and Technology 30 13-18.

[6] Bear, J. *Dynamics of Fluids in Porous Media*, Dover Publications Inc. New York NY. (1972).

[7] Orr, F.M., Scriven, L.E., Rivas, A.P., (1975) J. Fluid Mech. 67 723–742.

[8] Novy, R.A., Toledo, P.G., Davis, H.T., Scriven L.E., (1989) Chem. Eng. Sci. 44 1785-1797.

[9] Romero, L.A., Yost, F.G., (1996) J. Fluid Mech. 322 109–129.

[10] Rye, R.R., Yost, F.G., O′Toole, E.J., (1998) Langmuir 14 3937–3943.

[11] J.L. Vazquez, *The porous medium equation - Mathematical theory* Oxford Mathematical Monographs (2006)

[12] M.J.Baines, M.E.Hubbard, P.K.Jimack, (2011) Comm. Comput. Phys. 10 509–576..

[13] Alshibli, K.A., Alsaleh, M.I., (2004) J. Comput. Civil Eng. 18 36–45.

[14] Reemtsma, T., Quintana, J.B., Rodil, R., Garcia-Lopez, M., Rodriguez, I., (2008) Trends Anal. Chem. 27 727–737.

[15] The Center for Research Information, Inc., 9300 Brookville Rd, Silver Spring, MD 20910, +1 (301) 346-6501, http:// www.medresearchnow.com, cri@ix.netcom.com, *Health Effects of Trioctyl Phosphate* Contract No. IOM-2794-04-001 of the the National Academies (2004).

[16] Willett, C.D., Adams, M.J., Johnson, S.A., Seville, J.P.K., (2000) Langmuir 16 9396–9405.

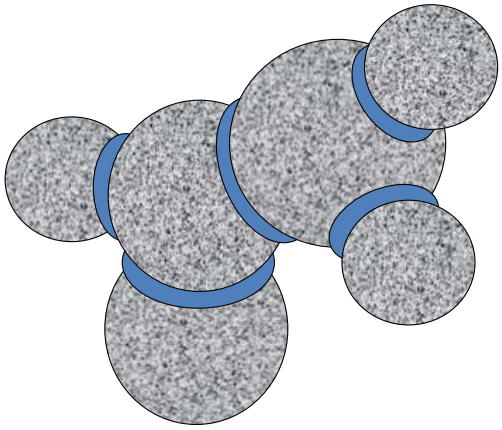

Figure 1: Illustration of the pendular ring regime at low levels of saturation.

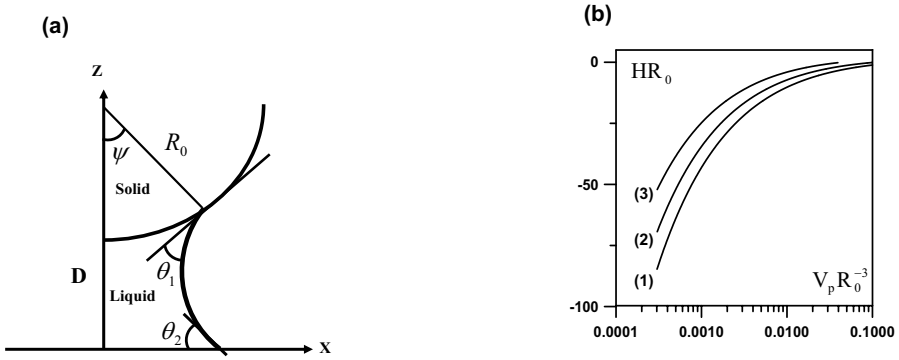

Figure 2: (a) Definition sketch for the pendular ring problem. (b) Typical dependences of the mean curvature H on the pendular ring volume V_p at $D = 0$, $\theta_2 = \pi/2$ and different values of parameter θ_1. (1) $\theta_1 = 0$, (2) $\theta_1 = \pi/6$, (3) $\theta_1 = \pi/4$.

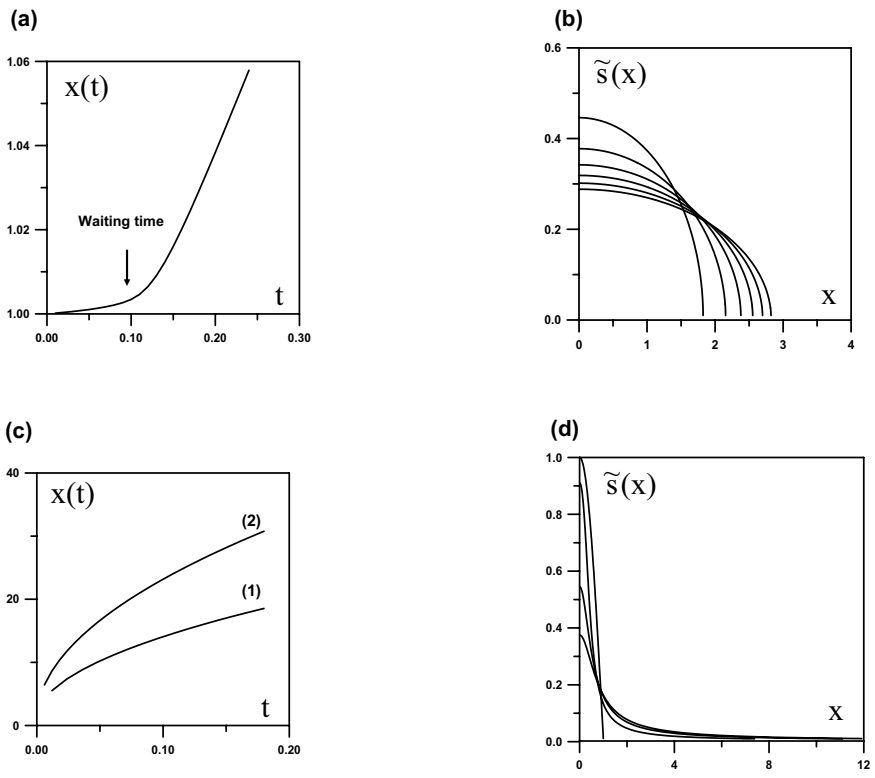

Figure 3: Numerical solutions of (6) at $D_0 = 1$. (a) Propagation front $x(t)$ for PME, $\gamma = 2$, at $s_F = 10^{-2}$, (b) Distributions $\tilde{s}(x,t)$ at different times $t > 0$ for PME at $s_F = 10^{-2}$, (c) Propagation front $x(t)$ for SFDE, $\gamma = -0.5$, at (1) $s_F = 10^{-2}$ and (2) $s_F = 5 \times 10^{-3}$, (d) Distributions $\tilde{s}(x,t)$ at different times $t > 0$ for SFDE at $s_F = 10^{-2}$.

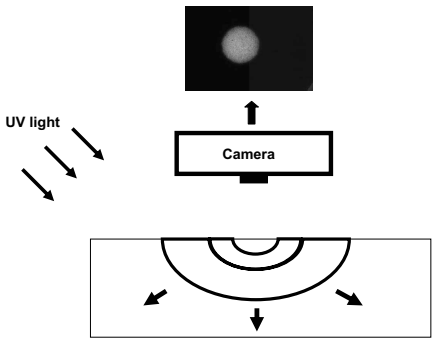

Figure 4: Illustration of the experimental setup and a typical wetted area image

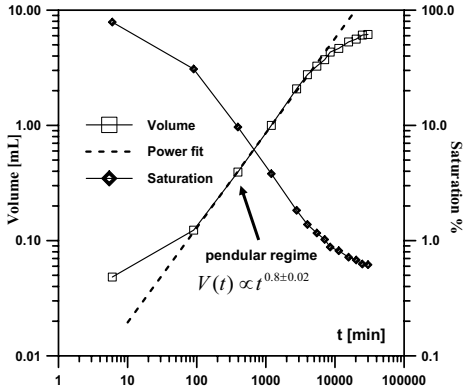

Figure 5: Typical spreading of an 11 microliter TEHP liquid drop in sand illustrated by evolution of the mean saturation and the wetted volume as a function of time.

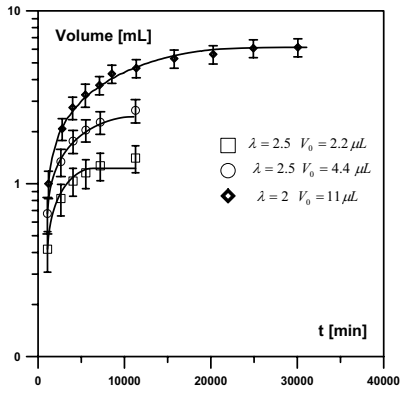

Figure 6: Evolution of the wetted volume $V(t)$ of TEHP liquid in sand as a function of time for different initial volumes of drops V_0. The numerical results are shown by solid lines, while experimental values are associated with symbols.